Liquid Crystals
Publication details, including instructions for authors and subscription information:
http://www.informaworld.com/smpp/title~content=t713926090

Crystallization kinetics study on N-(p-n-alkyloxybenzylidene)-p-n-alkylanilines (nO.m compounds)

P. A. Kumar; M. L. N. Madhu Mohan; V. G. K. M. Pisipati

Online publication date: 06 August 2010

To cite this Article Kumar, P. A. , Mohan, M. L. N. Madhu and Pisipati, V. G. K. M.(2000) 'Crystallization kinetics study on N-(p-n-alkyloxybenzylidene)-p-n-alkylanilines (nO.m compounds)', Liquid Crystals, 27: 6, 727 — 735
To link to this Article: DOI: 10.1080/026782900202192
URL: http://dx.doi.org/10.1080/026782900202192

LIQUID CRYSTALS, 2000, VOL. 27, NO. 6, 727–735

Crystallization kinetics study on *N*-(*p*-*n*-alkyloxybenzylidene)-*p*-*n*-alkylanilines (*n*O.*m* compounds)

P. A. KUMAR, M. L. N. MADHU MOHAN and V. G. K. M. PISIPATI*

Centre for Liquid Crystal Research and Education, Faculty of Physical Sciences, Nagarjuna University, Nagarjuna Nagar, 522 510 India

(*Received 28 July 1999; in final form 16 November 1999; accepted 17 November 1999*)

A comparative systematic kinetic study of crystallization among various smectogens of higher homologues of the benzylidene aniline *n*O.*m* series (9O.2, 13O.2, 14O.2, 15O.2, 16O.2, 2O.16, 11O.16, 16O.16 and 18O.16) has been carried out by thermal microscopy and differential scanning calorimetry (DSC). The DSC thermograms were run from crystallization temperature to the isotropic melt for different time interval. The liquid crystalline behaviour together with rate of crystallization of smectic ordering in newly synthesized *n*O.*m* compounds (16O.2, 2O.16, 11O.16, 16O.16, 18O.16) with respect to their lower homologues are discussed in relation to the kinetophase (which occurs prior to the crystallization), end chain lengths, the odd–even effect and chain length ratio. The molecular mechanism and dimensionality in the crystal growth were computed from the Avrami equation. The characteristic crystallization time (t^*) at each crystallization temperature was deduced from the individual plots of $\log t$ vs. ΔH. Further, a qualitative approach was made to the crystallization process in smectic layers.

1. Introduction

Rod-like molecules in smectic orderings, which are known to be arranged in equidistant planes with distinct orientational order of the molecular long axes, apparently leads to the formation of various smectic mesophases. In other words, the molecules in the orthogonal smectic phases are parallel to each other with their long axes perpendicular to the layer plane, resulting in free rotation of the molecules around the long molecular axis [1]. Consequently, in the case of a tilted phase the significant difference is the tilt of the molecular long axes with respect to the layer normal, leading to the hindered rotation of the molecule along the long axis [1]. Moreover, the layer thickness in a tilted mesophase is smaller than the molecular length while in the case of orthogonal ordering they are approximately equal. This degree of variation in the layer thickness, together with molecular rotation, has a striking influence on the rate of crystallization. In fact, the distribution of heat transformation in both orderings, which has a direct impact on the rate of crystallization, is a rather complicated process which may be elucidated structurally by detailed X-ray investigation. Alternatively, the study of crystallization kinetics [2, 3] is a powerful tool for addressing the crystallization mechanism in these orderings. Recently, Ziru *et al.* reported [4] the experimental results of kinetic studies on a discotic liquid crystal, and proposed a theoretical model for the process of crystallization in a columnar layer. Considering the scope of the crystallization behaviour in smectic layers, we are motivated to apply their experimental methods to yet another fascinating class of lamellar mesogens, the *n*O.*m* benzylidine aniline compounds.

The liquid crystalline materials belonging to the class of benzylidine anilines (usually known as *n*O.*m* compounds) exhibit fascinating mesomorphic behaviour associated with a distinct molecular ordering; the convenient working thermal ranges made them suitable members for systematic kinetic investigations. Our earlier research experience [5–9] with *n*O.*m* type compounds, involving various characterization techniques (dilatometric, dielectric and optical studies), has led us to a new chapter in the systematic study of crystallization kinetics for this series. This paper deals with kinetic investigations on a number of tilted and orthogonal members of *n*O.*m* liquid crystals which have recently been synthesized in this laboratory. The compounds studied fall broadly into two categories: *n*O.2 and *n*O.16 (figure 1). The former series comprises non-tilted kinetophases while most of the members of the latter series exhibit tilted kinetophases. A qualitative interpretation of these experimental findings has been developed.

*Author for correspondence;
e-mail: venkata_pisipati@hotmail.com

Liquid Crystals ISSN 0267-8292 print/ISSN 1366-5855 online © 2000 Taylor & Francis Ltd
http://www.tandf.co.uk/journals

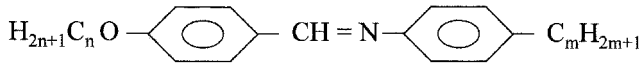

m = 2; n = 9, 13, 14, 15, 16
m = 16; n = 2, 11, 16, 18

Figure 1. Molecular structure of *n*O.*m* compounds.

2. Experimental

The *n*O.*m* compounds of the present study were synthesized and characterized as reported earlier [5]. The crystallization kinetics of the present compounds, determined by the rate of growth of a particular transition, were performed on a Perkin-Elmer DSC-7 differential scanning calorimeter. Further, the thermograms at each crystallization temperature, together with simultaneous phase identification [10], were obtained using a Mettler Toledo DSC (equipped with FP 99A central processor) supplemented by a Hertel and Reuss polarizing microscope. The DSC measurements were performed on each member of pure *n*O.*m* compound (3–5 mg sample) using aluminum and/or glass crucibles. A typical DSC scan for a given sample at each crystallization temperature is described as follows. The sample was heated to its isotropic melt with a scanning rate of 10°C min^{-1}; after holding for ~2 min to attain thermal equilibrium, the sample was cooled at the same scan rate to its predetermined crystallization temperature. After holding for a requisite time interval at crystallization temperature, the endotherm peaks were recorded while the sample was heated to the isotropic state at 10°C min^{-1}. This process was repeated for each individual member of the *n*O.*m* series at the appropriate preselected crystallization temperatures.

3. Results and discussion

3.1. *Phase identification*

The observed phase variants, transition temperatures and corresponding enthalpy values, obtained by thermal microscopy and DSC are presented in table 1. The compounds of the present *n*O.*m* series were found to exhibit characteristic textures [10], viz. focal-conic fan texture in the smectic A phase (2O.16), the appearance of transient transition bars across the focal-conic fans in the smectic B phase (*n*O.2), broken focal-conic texture in the smectic F phase (11O.16 and 16O.16) and mosaic texture in the G phase (18O.16). Further, the phase transition temperatures observed by thermal microscopy were found to be in good agreement with those from the DSC thermograms (table 1).

3.2. *Selection of thermal range of crystallization temperatures*

The procedure for the thermal selectivity of crystallization temperatures (CT) is described for 13O.2 as a representative member of the present series. The DSC thermograms of 13O.2 are illustrated in figure 2; the compound exhibited two distinct transitions in the heating cycle at 71.3 and 77.0°C, with heats of transition 66.7 and 11.3 J g^{-1}, respectively. The former transition

Table 1. Transition temperatures (in °C) from TM and DSC of *n*O.*m* compounds. Corresponding enthalpy values (in J g^{-1}) are given in brackets.

*n*O.*m*	Transition	TM	DSC
9O.2	I–SmA	71.1	70.4 (18.8)
	SmA–SmB	61.5	60.7 (9.7)
	SmB–Cr	40.6	35.9 (81.1)
13O.2	I–SmA	73.8	72.8 (10.9)
	SmA–SmB	65.1	64.3 (3.8)
	SmB–Cr	54.4	51.2 (73.4)
14O.2	I–SmA	75.9	75.1 (19.1)
	SmA–SmB	67.5	66.8 (9.0)
	SmB–Cr	55.2	54.8 (88.5)
15O.2	I–SmA	74.3	72.9 (16.4)
	SmA–SmB	68.2	67.8 (9.3)
	SmB–Cr	65.2	65.3 (110.9)
16O.2	I–SmA	73.5	72.4 (6.5)
	SmA–SmB	69.9	68.4 (9.1)
	SmB–Cr	64.5	63.1 (46.8)
2O.16	I–SmA	70.1	69.1 (4.8)
	SmA–Cr	52.2	49.0 (101.4)
11O.16	I–SmF	81.5	79.5 (14.3)
	SmF–Cr	45.8	44.3 (71.8)
16O.16	I–SmF	83.4	81.4 (25.5)
	SmF–Cr	63.4	62.1 (60.1)
18O.16	I–G	87.2	86.8 (45.8)
	G–Cr	56.8	56.3 (81.9)

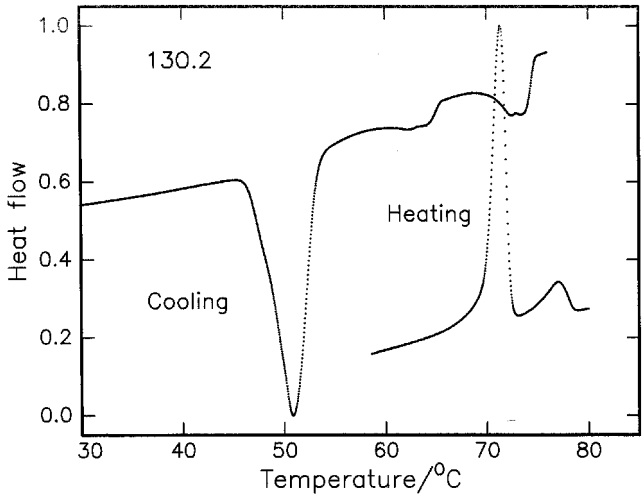

Figure 2. DSC heating and subsequent cooling thermograms of 13O.2 recorded at a scan rate of 5°C min^{-1}.

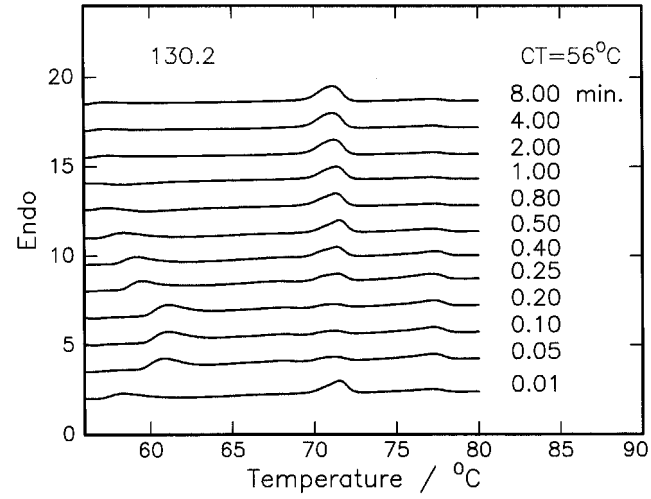

Figure 3. DSC endotherm profiles of 13O.2 at 56°C for different time intervals.

is identified as $T_{Cr\text{-}melt}$, the latter as $T_{SmA\text{-}I}$. Upon cooling, the transitions $T_{I\text{-}SmA}$, $T_{SmA\text{-}SmB}$ $T_{SmB\text{-}Cr}$, are observed at 72.8, 64.3 and 51.2°C with the corresponding enthalpies 10.9, 3.8 and 73.4 J g^{-1}, respectively. In the heating cycle the non-existence of a SmA–SmB transition implies the monotropic nature of the SmB phase. Similar patterns of monotropic transitions are observed in compounds 14O.2, 15O.2 and 16O.2. Figure 2 reveals the thermal span of the mesomorphic phases as: $(T_{Cr\text{-}melt})$–$(T_{SmB\text{-}Cr})$ = 20.0°C. Once the $T_{SmA\text{-}SmB}$ was completed, the kinetics of the crystallization from SmB could be investigated over the temperature range between $T_{SmA\text{-}SmB}$ and $T_{SmB\text{-}Cr}$; if the crystallization kinetics were not too fast. It is worth mentioning that there is a temperature range before the SmA–SmB phase transition which is below the crystal melting temperature at $T_{Cr\text{-}melt}$. The significance of its existence is, however, reflected by the appearance of this transition in the heating runs from predetermined crystallization temperatures.

The crystallization kinetics relating to the phase transformation from SmB to the melt is selectively performed at each predetermined crystallization temperature, viz. 55, 56, 57, 58, 59, 60 and 62°C. Typical DSC endotherm profiles for different time intervals at two crystallization temperatures, 56 and 62°C are illustrated in figures 3 and 4. The sample is held at 56°C for different time intervals (0.01 to 8.00 min) as indicated in figure 3. The heating curve with a crystallization time of $t = 0$ min is recorded immediately following the quenching of crystal to melt, at the crystallization temperature 56°C. This curve displays only the SmA–to isotropic endotherm indicating that the SmB to SmA transition has not yet occurred. However, at $t = 0.01$ min the appearance of a small peak is attributed to a SmB to SmA transition,

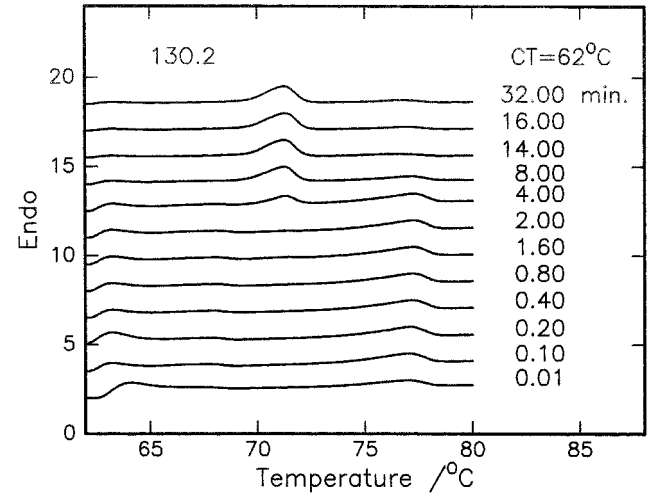

Figure 4. DSC endotherm profiles of 13O.2 at 62°C for different time intervals.

suggesting fast crystallization kinetics. Formation of the SmB phase increases with increase in time interval. This increase of the small peak continues until time interval reaches 0.40 min. At the same time interval, the endotherm shows the crystal to melting transition at 71°C. This endotherm at $t = 0.40$ min is critical in showing the simultaneous quenching of the SmB to SmA transition and the occurrence of the crystal to melting transition. The formation of a larger and larger crystal fraction, with time, from the SmB is reflected by a continuous increase of the crystal melting endotherm at the expense of SmB endotherm. This conversion process appears to be completed after 8 min, at which time the SmB endotherm peak could no longer be seen. This is further substantiated by the saturated value of enthalpy of the endotherm

profile at 71°C, corresponding to the melting transition after 8 min. Moreover, quenching of the SmB mesophase requires longer time intervals for crystallization temperatures above 56°C. An interesting feature is the appearance of a shoulder on the higher temperature side of the crystal melting endotherm which become more prominent with time. This is perhaps due to a crystalline phase transformation leading to a structural evolution with time.

The enthalpy values for individual transitions at different time intervals were calculated at each crystallization temperature, and the corresponding data plotted against the corresponding logarithm of time intervals for each member of the *n*O.*m* series. Figure 5 shows plots for crystallization of 9O.2 (as a representative case) at 43 and 53°C; these plots have an identical shape, apart from the shift in the log *t* axis suggesting the limitations of the rate of crystallization kinetics [4]. Moreover, simultaneous measurement of the heats of melting of the SmB endotherm with time shows, without ambiguity, that the effective beginning and end of the crystal formation process coincide with those of the decay of the SmB phase, illustrating a direct SmA to crystal phase conversion.

A plot of heats of melting of the mesomorphic phase vs. the log of annealing time for different crystallization temperatures of 9O.2, obtained by shifting data along the log *t* axis to the 53°C curve, is depicted in figure 6. Such a master curve strongly suggests that the same mechanism operates for crystallization from both the SmA and SmB phases. As expected [4], the overall crystallization rate is controlled by a nucleation rate influencing the rate of growth of domains; this is a function of the degree of supercooling and the starting smectic mesophase.

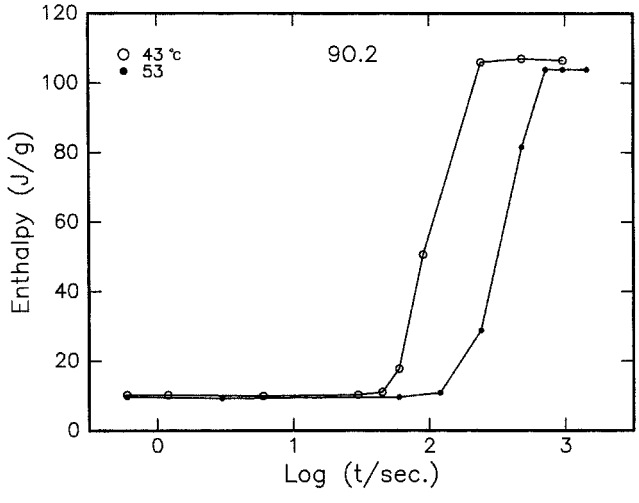

Figure 5. Heats of melting as a function of the logarithm of annealing time in the SmB of 9O.2 at 43 and 53°C.

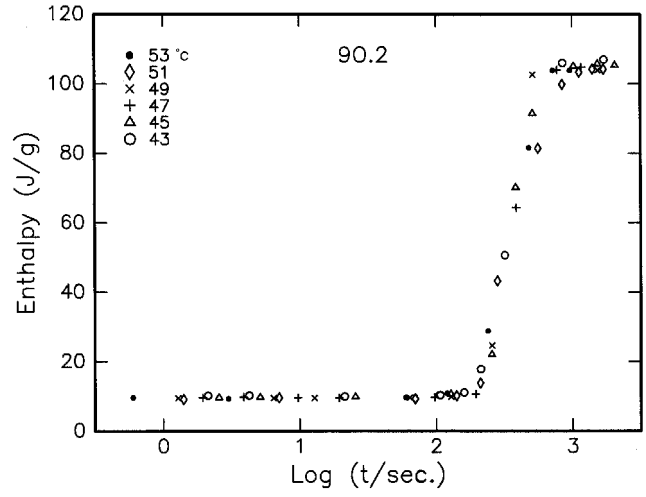

Figure 6. Plot of heats of melting of the mesomorphic phase of 9O.2 vs. the log of the annealing time for different temperatures, obtained by shifting data along the log *t* axis to the 53°C curve.

Similar experimental studies were carried out for measurement of the crystallization kinetics of the remaining *n*O.*m* series. The corresponding data of crystallization time *t** along with the calculated crystal growth parameters for different crystallization temperatures are summarized in table 2, which includes results relevant to the following sections.

3.3. *The process of crystallization*

In general, the kinetics of crystallization involving the rate of growth of small domains in a smectic phase is manifested equally by its temperature and time. Temperature dependent nucleation, taking place as a homogeneous process over a constant period of time, leads to the phenomenon of sporadic growth. In addition, defects and impurities in the compound have a pronounced influence on the nucleation process [4]. Further contributions from solid state transformations, where growth occurs only at the surface of the nuclei, hampers the overall rate of phase transformation and the dimensional geometry of the growing domains.

It is well known that the crystallization process involving the fraction of the transformed volume x, at a time t measured since the beginning of the crystallization process, is described by the Avrami equation [2, 3]

$$x = 1 - \exp(-bt^n) \qquad (1)$$

where the constants b and n depend on the nucleation mechanism and the dimensional geometry of the growing domains, respectively. The transformed volume x at a crystallization time t is given by $\Delta H/\Delta H_0$, where ΔH is the crystal heat of melting measured at time t and ΔH_0 is the maximum value obtained from the plateau of individual master curves (figure 6).

Table 2. Measured crystallization parameters for 63.0% transformation (by volume) from the various smectic mesophases to the crystalline phase of a number of *n*O.*m* compounds.

*n*O.*m*[a]	Crystallization temperature/°C	*t**/min	*x*	*n*	*b*
9O.2	43	3.0	0.994	5.27	6.70×10^{-5}
	45	6.0	0.995	5.32	7.20×10^{-5}
	47	6.0	0.996	5.66	3.97×10^{-5}
	49	12.0	0.991	4.81	6.41×10^{-6}
	51	12.0	0.994	5.25	2.16×10^{-6}
13O.2	55	2.0	0.993	5.10	3.68×10^{-3}
	56	4.0	0.993	5.10	8.50×10^{-4}
	57	4.0	0.993	5.09	8.50×10^{-4}
	58	6.0	0.989	4.58	2.72×10^{-4}
	59	8.0	0.994	5.17	4.66×10^{-4}
	60	9.0	0.994	5.17	1.16×10^{-5}
	62	16.0	0.993	5.10	7.20×10^{-7}
14O.2	54	1.8	0.995	5.32	4.57×10^{-2}
	56	2.0	0.994	5.25	2.50×10^{-2}
	58	8.0	0.993	5.32	1.81×10^{-5}
	60	16.0	0.994	5.25	3.90×10^{-7}
	62	18.0	0.997	5.35	3.82×10^{-7}
15O.2	67	1.0	0.996	5.00	9.70×10^{-1}
	68	2.0	0.993	5.00	3.10×10^{-2}
	69	4.0	0.999	5.11	9.70×10^{-4}
	70	12.0	0.992	4.99	3.05×10^{-5}
	71	14.0	0.997	5.03	1.86×10^{-6}
	72	16.0	0.998	5.22	9.50×10^{-7}
2O.16	54	1.0	0.998	6.32	1.25×10^{-2}
	55	2.0	0.993	5.00	0.97×10^{-3}
	57	12.0	0.996	5.53	1.05×10^{-6}
	58	48.0	0.994	5.25	1.42×10^{-9}
11O.16	48	6.0	0.996	5.66	1.28×10^{-4}
	50	8.0	0.997	5.79	3.09×10^{-5}
	52	20.0	0.998	6.57	3.12×10^{-6}
	54	60.0	0.999	5.75	1.28×10^{-9}
	56	80.0	0.991	4.81	3.05×10^{-10}

[a] The melting transitions corresponding to 16O.2, 16O.16 and 18O.16 are not well resolved.

If the kinetics of crystallization from the corresponding smectic phases are described by the above Avrami equation, the data for all the crystallization temperatures can be applied to the single equation [4]

$$x = 1 - \exp[-(t/t^*)^n] \qquad (2)$$

where $t^* = b^{-1/n}$. Further, the characteristic time t^* can be experimentally determined, since at $t = t^*$, $x = 0.632$. Substituting these values of t^* and x in equation (1), constants b and n are obtained at a specified crystallization temperature. It is found that the constant n (the dimensional geometry of the growing domains) is unaltered with a value of ~ 5.0 while the magnitude of the constant b, which governs the nucleation mechanism, varies in the order 10^{-1} to 10^{-7} for all the compounds of *n*O.2 series. This trend in the magnitudes of the two constants is, however, inconsistent with the data reported for discotic [4] and smectic [11] mesophases. A possible explanation for the magnitude of n is supplied by either sporadic nucleation and growth in two dimensions or by growth in three dimensions. The former is more favourable for crystallization to occur in smectic liquid crystals while the latter argument is extremely unlikely.

A quantitative approach has been made to a description of the crystallization behaviour in terms of the varied magnitudes of constant b with respect to crystallization temperatures by constructing a plot (figure 7) of $\log b$ at different crystallization temperatures for all the compounds of the *n*O.2 series. As expected, the magnitude of constant b increases as the crystallization temperature decreases. The corresponding slope values for each member of the *n*O.2 series is obtained by a linear fit which is performed to the respective values of $\log b$ and crystallization temperatures. Figure 7 shows an interesting increasing trend in the magnitude of slopes corresponding to compounds 9O.2, 13O.2, 14O.2 and 15O.2. In other words, it has been observed that the alkyloxy chain length has a pronounced influence on the nucleation mechanism. The range of crystallization temperatures of the series narrows with increase of the alkyloxy chain length. The influence of the alkyloxy chain length in a particular *n*O.*m* series on the rate of crystallization will be discussed in detail in the following section.

3.4. *Influence of phase variant on crystallization kinetics*

In general, the phase sequence in liquid crystal materials has a pronounced influence on their crystallization kinetics. In fact the 'kinetophase', which occurs prior to crystallization, is solely responsible for many combinational

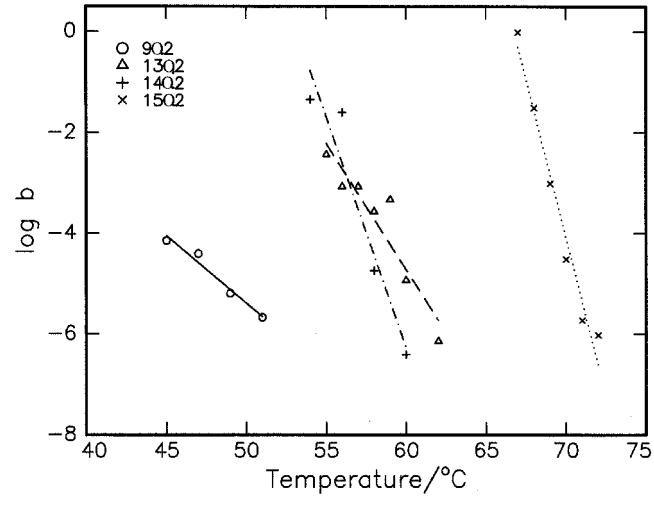

Figure 7. The logarithm of the constant b as a function of crystallization temperature for the *n*O.2 compounds.

factors of the crystallization mechanism. Our experimental studies on different *n*O.*m* compounds exhibiting various kinetophases enabled us to arrange them in increasing order of their crystallization time in orthogonal and tilted kinetophases:

SmB < SmA
G < SmF < SmI < SmC.

This order clearly implies that the rate of crystallization is fast for kinetophases close to the crystalline phase. That is, crystallization becomes slow for kinetophases near the isotropic melt. It is interesting to add that this order remains unaltered for both tilted and orthogonal kinetophases. A detailed discussion of the qualitative approach leading to the molecular contributions will be presented in the following sections.

The crystallization behaviour of different kinetophases (tilted/orthogonal) was investigated for selected members of the *n*O.*m* series. For this purpose, the selection of individual compounds was made in such a way as to give: (a) a minimum of two compounds exhibiting different kinetophases for each class of tilted/orthogonal ordering; (b) successive kinetophases among the individual class of tilted/orthogonal orderings. The former condition provides substantial information regarding crystallization kinetics among the two different orderings, while the latter condition establishes a sequential order of kinetophases in each category. In addition to the above selection conditions, all the compounds studied fell into either the *n*O.2 or *n*O.16 series, which in turn facilitated estimation of the contribution of the alkyloxy chain length. Thus, the selection of the kinetophases in terms of compounds can be represented as:

orthogonal kinetophases: SmA (2O.16) and SmB (nO.2)
tilted kinetophases: SmF (11O.16, 16O.16) and G (18O.16).

3.5. *Kinetics of SmA and SmB kinetophases*

The characteristic crystallization times (t^*), along with other parameters of the individual members of SmA and SmB kinetophases are summarized in table 2. As predicted, the data revealed that the crystallization time for 2O.16, involving the SmA kinetophase, is longer than those for the *n*O.2 series exhibiting the SmB kinetophase. Further, the similar trend in the variation of the slopes of *n*O.2 compounds (figure 7) is observed to be higher than for compound 2O.16, strongly suggesting a faster nucleation mechanism in the *n*O.2 compounds.

3.6. *Influence of alkyloxy carbons in nO.2 compounds*

We have performed a systematic kinetic studies on the *n*O.2 compounds, in order to study the effect of end chain lengths on the crystallization process; all the members of this series have the same kinetophase (SmB).

Comparative studies were performed for compounds 9O.2, 13O.2, 14O.2 and 15O.2. The data (table 1) suggest that the crystallization thermal range among these compounds decreases from 14 to 5°C with increase in the alkyloxy carbon number, with an exception in the case of 14O.2 (11°C). This interrupted trend is, however, accounted for by the odd–even carbon chain lengths of the alkoxide moiety. However, as expected, the isotropic clearing point shifts to higher temperatures with increase in the carbon chain length. From this experimental evidence one can clearly rule out the influence of an odd–even effect; on the other hand, it has a striking role on other mesomorphic properties. It is worth adding that there is a sequential increasing trend in the thermal ranges of compounds *n*O.2 (when *n* is odd): for instance, the final crystallization temperature of 9O.2 (CT = 55°C) will be the initial crystallization temperature for the subsequent compound (13O.2) of the series. This interesting trend can be substantiated by the difference in the thermal range of the unique kinetophase (SmB) among various compounds. Further, it is evident that the degree of variation of the dimensionality parameter *n* with respect to the carbon number is found to be of the order ~ 5.0, which in turn infers a unique crystallization mechanism for the *n*O.2 series. A possible explanation for the crystallization dimensionality is a sporadic nucleation and growth involving a homogeneous process of continuous nucleation over a constant time [4]. Furthermore, the volume transformation ($x = \Delta H/\Delta H_0$) calculated at individual crystallization time t^*, and in accordance with the equation (2), after the completion of 63% transformation from smectic mesogen to the crystalline phase, strongly implies the completion of the crystallization process.

3.7. *Kinetics of the SmF and G kinetophases*

The mechanism of crystal growth in the tilted hexatic phases was studied for SmF (11O.16 and 16O.16) and G (18O.16) kinetophases. As shown by the data (table 1) the crystallization kinetics is found to be slow when compared with the orthogonal orthorhombic kinetophases. This is best explained on the basis of our well established kinetophase sequential order; these tilted phases fall far from the crystal end of the sequence, thus promoting slow crystallization. This positional sequential effect is also reflected in the intra-hexatic kinetophases: the experimental data for 11O.16 and 16O.16 which exhibit SmF kinetophases, suggest a slower crystallization process than for 18O.16 which shows a G kinetophase. This is also in concurrence with our previously discussed results where the rate of crystallization is independent of numbers of alkyl/alkyloxy carbons, provided the kinetophase is different.

3.8. *Effect of alkyloxy chain length in nO.16 compounds*

Crystallization modifications among the class of similar *n*O.16 compounds with the same kinetophase were studied on compounds 11O.16 and 16O.16, investigating the significant role of alkyloxy end chains. The experimental data for these two compounds suggest that the crystallization time t^* increases with increasing alkyloxy chain length. This trend is found to be in the reverse order when compared with the kinetics of *n*O.2 compounds where the crystallization time becomes shorter for the higher analogues. No attempt has been made at this stage to explain this interesting opposite kinetic trend from molecular considerations. The endotherm profiles of 11O.16 (figure 8) and 16O.16 (figure 9) at crystallization temperatures 52 and 67°C, respectively, clearly show a doubling in the nature of the melting transition. This may be attributed to the existence of two equal molecular fragments of the compound at the said crystallization temperatures. Further, it is found that the crystallization thermal range for these compounds has decreases from 28 to ~ 9°C with the increase of alkyloxy carbon number. On the other hand, as expected, the isotropic clearing point increases with the increase in the carbon chain length. The unaltered values of the dimensionality parameter ($n \simeq 5.0$), after the completion of 63% transformation from the respective kinetophase, strongly suggest that the crystallization mechanism is completed through a unique process of continuous nucleation over a constant time [4].

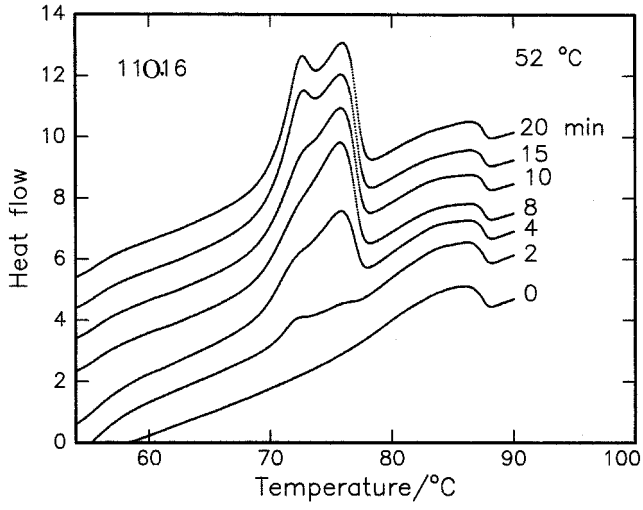

Figure 8. DSC heating curves for 11O.16 at 52°C for different time intervals.

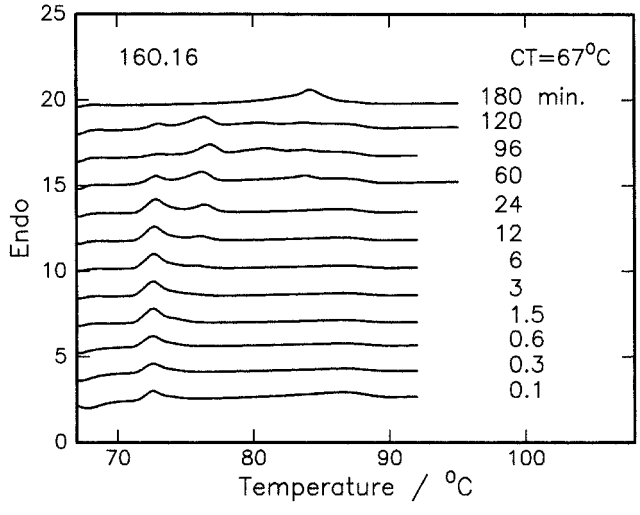

Figure 9. DSC heating curves for 16O.16 at 67°C for different time intervals.

3.9. *Influence of the n/m ratio*

Apart from the significant role of kinetophase variant, the ratio between the alkyloxy and alkyl end chain lengths (n/m) has a pronounced influence on the rate of crystallization. Our systematic studies on the present series of *n*O.*m* compounds also points our attention in this direction and we established the following effects related to n/m ratio.

(1) Irrespective of the kinetophase, the alkyl chain length dominates the crystallization time in the *n*O.16 series leading to a slow kinetic rate. When n/m reaches unity or more (18O.16) the crystallization time becomes shorter.

(2) The crystallization time reaches its maximum value (slow rate of crystallization) for a compound in a particular series when the chain lengths of both alkoxy and alkyl carbons are equal ($n = m$) (12O.12, 14O.14 and 16O.16).

(3) A sudden reversal in the kinetic rate takes place when a slight inbalance occurs in the n/m ratio due to an increment in the alkyloxy (n) chain (18O.16). At this juncture, one can easily rule out the role of alkyl chain length on the rate of crystallization.

Thus, the experimental results on *n*O.16 compounds show altogether a different trend in the crystallization mechanism, since the increase in alkoxy chain length has a negligible influence. This dominating role of alkyl chain over alkoxy chain length on the rate of crystallization may be explained in terms of the kinetophase. When we proceed from 2O.16 ($n/m < 1$) to 16O.16 ($n = m$) and further (except 2O.16), these compounds all exhibit a tilted kinetophase of either F or G type. Our preliminary investigations on other series, viz. *n*O.12 and *n*O.14, showed the expected trend of slow crystallization when $n = m$. This, however, can not be verified in the case of *n*O.2 compounds as 2O.2 is a non-liquid crystal compound.

Figure 10 gives plots of crystallization time vs. *n/m* ratio for compounds of the *n*O.2 and *n*O.16 series showing the role of end chains on the rate of crystallization. From this figure we can say that:

(1) the curves are not symmetrical;
(2) the shapes of the two curves are independent of one another;
(3) the curves indicate the expected trend for the remaining series of *n*O.*m* compounds which will fall between the two extremes;
(4) the curve for the *n*O.8 series is expected to be symmetric.

3.10. *Crystal growth and nucleation mechanism*

In this concluding section we make a qualitative approach to an understanding of the nucleation process in the smectogens of both the tilted and orthogonal categories. Apart from the molecular contributions which strongly affect the nucleation process in tilted and orthogonal kinetophases, we still have a reasonable qualitative approach in addressing the crystallization mechanism at the micro level of the smectic layers. According to recent work of Ziru and co-workers [4] on crystallization kinetics in discotic phases, the intercolumnar distance in a two dimensional crystal is a dominating factor in the crystal growth mechanism. In accord with their view of crystallization mechanism, we have extended similar structural changes to the smectogens under study.

As the temperature is lowered, in both the orderings, the formation of an ordered domain occurs which converts to a stable nucleus that initiates the aggregation of the surrounding molecules to form layered domains. The origin of the nucleus is critical since its formation proceeds until it reaches a sufficient size to initiate the crystallization process. At this juncture, it is proposed that this process of crystallization is controlled by either the lamellar or interlayer distances in non-tilted and tilted kinetophases, respectively. In such a process of seed nucleation, factors relating to the smectic layers play a crucial role. A particular molecule in the lower smectic layer first acquires the requisite energy to allow the formation of ordered domains, which in turn propagate crystallization in the adjacent smectic layers. These ordered domains will further proceed through the smectic layer by a process of successive addition of the molecules from neighbouring layers leading to sporadic nucleation and growth in two dimensions. This process continues until the crystallization is complete.

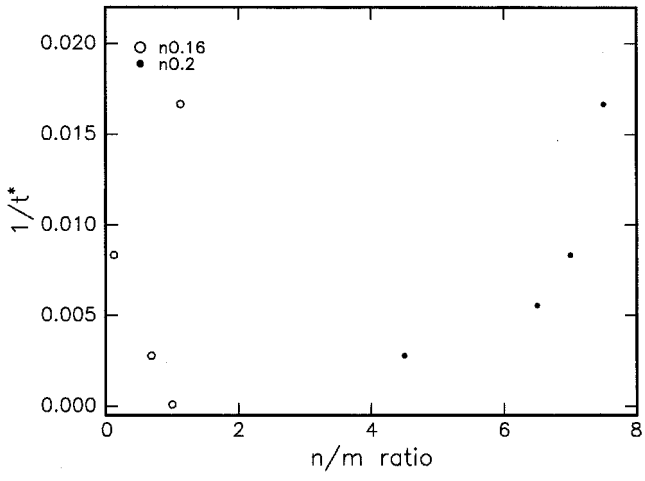

Figure 10. Plot of crystallization time t^* vs. *n/m* ratio for the *n*O.2 and *n*O.16 series.

This mode of conversion of the lamellar layer correlation in a tilted ordering is a rather complicated and slow process. On the contrary, in a non-tilted kinetophase the start of the crystallization process begins with the annihilation of short range forces and subsequent formation of new long range forces, triggering the rapid completion of the crystallization. These facts have been experimentally realized in the present study in terms of the delayed crystallization process in a tilted kinetophase as compared with that in the orthogonal kinetophase.

Furthermore, the constant b has a direct influence on the nucleation mechanism. It is found that b has a smaller value as the crystallization temperature decreases. Throughout the same kinetophase, the temperature dependence of constant b is as depicted in figure 7. The linear nature of the curves strongly implies a unique crystallization process among members of the *n*O.2 series. In *n*O.2 compounds the gradual increase of the slope of the $\log b$ curve (figure 7) with increasing alkyloxy chain length supports the high rate of crystallization, as discussed in the previous section. Nevertheless, the Avrami constants obtained in the present study are in reasonable agreement with those reported for discotic and smectic phases. The value of constant b in this study reaches the order of 10^{-7} which is two orders magnitude smaller and one order greater than those reported for smectogens [11, 12] and discotics [4], respectively. As evident from equation (2) the characteristic time t^* is inversely proportional to the constant b, and is directly proportional to the dimensionality constant n.

The authors are grateful to the Council of Scientific and Industrial Research (CSIR), Department of Atomic Energy (DAE) and Department of Science and Technology (DST), New Delhi, India for financial support.

References

[1] Demus, D., 1994, *Liquid Crystals: Phase Types Structures, and Chemistry of Liquid Crystals* (New York: Springer).

[2] Avrami, M., 1939, *J. chem. Phys.*, **7,** 1103.
[3] Avrami, M., 1940, *J. chem. Phys.*, **8,** 212.
[4] Ziru, H., Yue, Z., and Alain, C., 1997, *Liq. Cryst.*, **23,** 317.
[5] Rao, N. V. S., and Pisipati, V. G. K. M., 1983, *Phase Trans.*, **3,** 317.
[6] Rao, N. V. S., and Pisipati, V. G. K. M., 1983, *J. phys. Chem.*, **87,** 899.
[7] Srinivasulu, M., Potukuchi, D. M., and Pisipati, V. G. K. M., 1997, *Z. Naturforsch.*, **52a,** 713.
[8] Potukuchi, D. M., Rani, G. P., Srinivasulu, M., and Pisipati, V. G. K. M., 1998, *Mol. Cryst. liq. Cryst.*, **319,** 19.
[9] Rani, G. P., Potukuchi, D. M., and Pisipati, V. G. K. M., 1998, *Liq. Cryst.*, **25,** 589.
[10] Gray, G. W., and Goodby, J. W., 1982, *Smectic Liquid Crystals—Textures and Structures* (Leonard Hill, Heydon & Sons).
[11] Price, F. P., and Wendorff, J. H., 1971, *J. phys. Chem.*, **75,** 2849.
[12] Price, F. P., and Wendorff, J. H., 1972, *J. phys. Chem.*, **76,** 276.